Numerical Modeling of Surface Acoustic Wave for Silica Tapered Fiber

Hui Jing Lee, Fairuz Abdullah, and Aiman Ismail
Photonic Technologies Research Group, College of Engineering
Universiti Tenaga Nasional, 43000 Kajang, Selangor, Malaysia
LHJing@uniten.edu.my

***Abstract*—This paper presents the numerical modeling of optical and acoustic wave characterization for a tapered fiber with Finite Element Method. Result focuses on the evolution of surface acoustic wave in the fundamental mode and a higher order acoustic mode behavior of a tapered silica fiber with radius of 2 μm. Result also presents the difference in overlap integral for various fiber radius at different propagation constants. Also, the co-existence of surface acoustic wave and hybrid acoustic wave are simulated at fiber radius of 6 μm. A reliable modeling tool is developed to be utilized in Brillouin characterization for various fibers which is applicable in communication, sensor and amplifier.**

***Index Terms*—surface acoustic wave, tapered fiber, Stimulated Brillouin Scattering, Finite Element Method**

I. Introduction

Stimulated Brillouin Scattering (SBS) was firstly introduced in 1922, it is a nonlinear process where the acoustic vibration will scatter the injected pump wave to propagate in the backward direction which is commonly known as the Stoke wave and anti-Stoke wave [1]. One rule for the phenomenon to take place is that the injected pump power has to exceed the fiber threshold power. Acoustic wave forms with the combination of shear acoustic wave and longitudinal wave which is called hybrid acoustic wave (HAW) [2]. However, it is named as the surface acoustic wave (SAW) when the waves propagates on the fiber surface [3]. SAW means the superposition of longitudinal and shear waves propagating at the surface of an elastic solid. SAW travels in an elliptical motion, boundary condition for it to happen is that the normal force to the surface of fiber has to be zero. SAW occurs when the fiber is being shaken because of the interaction between guided wave and evanescent field [3]. The wave confines at the outer surface region of a medium and its penetration dept is inversely proportional to the frequency of light.

A tapered single mode fiber (TSMF) is being produced with the heating and stretching of a normal fiber. An ideal TSMF shall carry a few characteristics: has a tapered waist of 0.8 - 3.0 μm, uniform diameter along the fiber and a smooth tapering surface [4]. Mode field deformation is strictly prohibited for TSMF, hence any external force and mechanical stress are not allowed in the tapering process [5]. TSMF has been receiving great attention since the past decade in various application especially in the sensor application. TSMF is also applicable in refractive index based transducers [6] and for the surface plasmon resonance (SPR) transducers [7]. Optical propagation across TSMF was demonstrated in both experiment and simulation [8]. The sensitivity of tapered fiber for protein concentration detection was also successfully demonstrated [9].

The novel SAW propagation was reported by Beugnot for tapered fiber with 1 μm core diameter [3] . Result shows a high threshold power at 60 W, it is difficult for the injected pump wave to overcome the threshold power hence it is not plausible in SBS. It is also experimentally shown that the interaction of SAW with graphene oxide simulates the wide-band mode-locked pulses which is applicable in communication and sensing application [10]. Surface Brillouin Scattering was also experimentally shown for Titanium Carbide film [11]. Recent investigation focuses on the optical and acoustic wave interaction of suspended-core microstructured Chalcogenide fiber [12]. Realizing the gap in the extant literature, more research work is needed to investigate the potential of surface acoustic wave for TSMF in SBS.

There are several numerical methods which are feasible for fiber modeling such as Finite Element Method (FEM) [13], Mode Matching Method (MMM) [14], Finite Difference Frequency Domain (FDFD), Finite Difference Time Domain (FDTD), and Beam Propagation Method (BPM) with their own advantages and disadvantages [15]. FEM is a more promising method for fiber modeling because it is more accurate and powerful, most importantly it has a unique parameter to handle the penalty function at boundary of cable which involve different fiber materials. FEM is able to perform fine meshing for a more accurate fiber mapping, the only drawback is that the computation process is tedious and it involves long computation time [16].

This paper reports characterization of tapered fiber using FEM. Section II presents the fundamental of finite element method and how it is proposed to model the fiber. Section III then explains the theory and formulation of SBS. Result and discussion first presents both the fundamental and higher order of longitudinal and shear SAWs for silica microfiber with R = 2 μm at phase matched condition. It then plots the variation in optic-acoustic overlap factor of different fiber radius at different wavenumbers. In addition, result also presents the co-existence of optical and acoustic wave for R = 6 μm.

978-1-5090-1134-6/17/$31.00 ©2017 IEEE

II. Finite Element Method

Figure 1 simplifies the flow of FEM algorithm used in this research. There are few fundamental steps in FEM [17]: firstly the fiber structure has to adapt a suitable amount of meshing elements. Nodal points will be assigned at the boundary region of elements, then the element properties are solved using an interpolation function. Lastly, matrix equation using the variational approach is used to solve for the element properties. Based on Figure 1, it is crucial to ensure that the incremental step of meshes are within the tolerance range of boundary. For the case where the error is not within the range of tolerance, the incremental steps have to be redefined. Else, the incremental steps are being analyzed to solve for the element properties. In this research, the FEM algorithm is programmed in Fortran to solve for the fiber meshing. The nodal solution of the element properties are then solved using Matlab to generate the fundamental and higher order mode behavior.

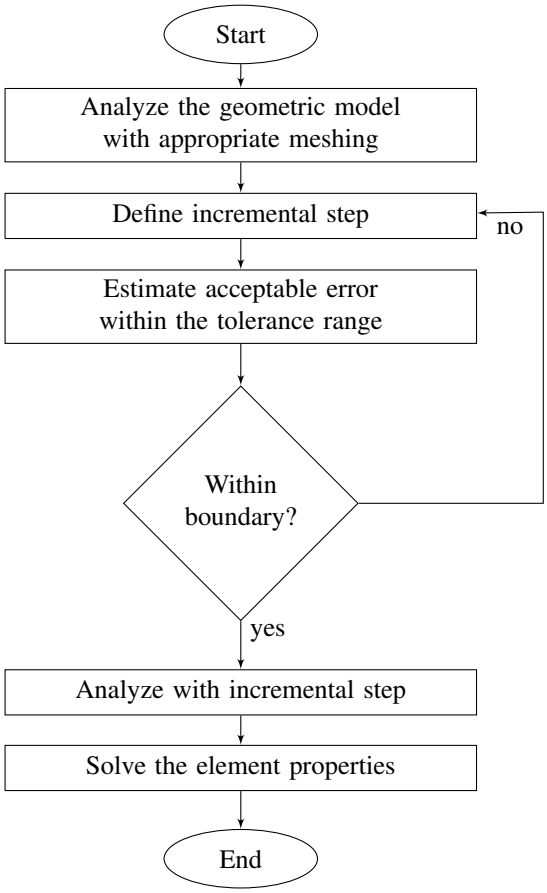

Figure 1: Flow of FEM algorithm

III. Stimulated Brillouin Scattering Formulation

In SBS, optical waveguides interact with the acoustic waveguides. At the phenomenon where the incident pump is more than the value of threshold power, acoustic wave will be generated. The reflective index of the fiber will fluctuate and scatter the injected pump wave, this will generate a Stoke wave propagating in the opposite direction. Power from the pump wave will be transfered to the Stoke wave and therefore scattering effect occurs. The property of optical mode can be expressed as:

$$\triangle_t^2 E + (\frac{2\pi}{\lambda})^2 (n^2 - n_{\text{eff}}^2) E = 0 \tag{1}$$

where $\triangle_t$ represents transverse Laplacian operator in both x and y plane, n_{eff} is the effective refractive index for fundamental optical mode, λ is the incidence wavelength, n signifies refractive index of fiber, and E represents the spatial distribution for optical field [18].

Hence, the optical wave propagation constant can be solved as:

$$\beta_{\text{optic}} = \frac{2\pi n_{\text{eff}}}{\lambda} \tag{2}$$

using n_{eff} and λ in Equation 1 [19].

The solution of acoustic wave behavior will depend on the optical wave propagation constant under a mode-matching condition. In SBS, the interaction between optical wave and acoustic wave implies the mathematical derivation of Braggs Grating formula. The refraction and reflection of wave vary at a different media interface:

$$k = 2\beta \tag{3}$$

which explains that backward scattering effect of acoustic wave will generate the propagation of Stoke wave [20]. The angular energy, ω and acoustic propagation constant, ak_{acoustic} parameters will then solve for the acoustic wave velocity, V_{ac}:

$$V_{ac} = \frac{\omega}{ak_{\text{acoustic}}} \tag{4}$$

Inserting the value of V_{ac} solved in Equation 4, the Brillouin shift for fundamental mode is therefore expressed as [21]:

$$v_B = \frac{2n_{\text{eff}} V_{ac}}{\lambda} \tag{5}$$

.

The shift in acoustic velocity, v_{ac} is solved:

$$V_{ac} = v_{ac} \sqrt{\frac{1}{v_1^2} - \frac{1}{v_2^2}} \tag{6}$$

where v_1 and v_2 represent the core and clad velocity, respectively.

The Brillouin gain spectrum (BGS) is calculated as:

$$g^{(m)}(v) = g_p \frac{\frac{\triangle v_{ac}^{(m)\,2}}{2}}{[v_s - (v_p - v_{ac}^{(m)})]^2 + \frac{\triangle v_{ac}^{(m)\,2}}{2}} \Gamma_{ij} \tag{7}$$

where v_p is the pump frequency and v_s is the Stoke frequency. Γ_{ij} represents the overlapping factor between optical wave and acoustic wave, $\triangle v_{ac}^{(m)}$ signifies the Full Width Half Maximum (FWHM) for m-th order of acoustic mode and $v_{ac}^{(m)}$ is the m-th order acoustic frequency shift. Then, Γ_{ij} is defined as:

$$\Gamma_{ij} = \frac{\int \left[\left| H_i^2(x,y) \right| \left| U_j(x,y) \right| \right]^2 dA}{\int \left| H_i(x,y) \right|^4 dA \int \left| U_j(x,y) \right|^2 dA} \tag{8}$$

where $U_j(x,y)$ is the acoustic wave displacement vector and $H_i(x,y)$ is the fundamental optical wave.

$v_{ac}^{(1)}$ is also expressed as v_B which is the Brillouin acoustic shift for fundamental mode wave behavior. The peak gain of Brillouin scattering, g_p is achieved when v_B is equivalent to the difference between pump frequency and stoke frequency:

$$g_B(v) = g_p = \frac{4\pi^3 n_{\text{eff}}^8 p_{12}^2}{c\lambda_p^3 \rho_o v_B \triangle v_B} \tag{9}$$

in which ρ_o signifies the fiber core density, p_{12} is the elasto-optic coefficient which contributes to the periodic light scattering, $\triangle v_B$ is the FWHM of acoustic wave, and c represents speed of light. [22].

Finally, substituting the peak gain of Brillouin Scattering will solve for the threshold power, P_{th}:

$$P_{th} = \frac{\kappa A_{\text{eff}}}{g_p L_{\text{eff}} K} \tag{10}$$

where the numerical factor, κ varies with the fiber length and is ≈ 21. A_{eff} signifies the effective area of fiber, the effective length of fiber, L_{eff} can be expressed as $\frac{1-e^{-\alpha L}}{\alpha}$. α represents the attenuation loss of fiber whereas K is the factor of wave polarization with a value of 1-2 [23].

IV. Results and Discussion

Table 1 lists the refractive index for the core and clad region for a standard silica fiber [2].

Table 1: Refractive index of silica fiber

Materials	Region	n
Silica Fiber	Core	1.4514
	Clad	1.4447

For a tapered fiber, the initial clad region of standard silica fiber will now function as the core and the outer air is defined to be the clad with n = 1.0. At the core region, shear velocity is 3677 m/s and logitudinal velocity is 5736 m/s. Air does not support shear propagation, it only propagates in the z direction with longitudinal velocity of 343 m/s [24]. Density of air is set at 1.225 kg/m^3 [25].

Figure 2 shows fundamental optical mode for a 2 μm core radius of TF. Result shows a strong optical confinement in the center core region. n_{eff} is recorded to be 1.4213 and beta propagation is 5.7736 μm^{-1}. In Figure 2 (d), 2d plot confirms optic confinement for TF with R = 2 μm. Figure 3 shows higher order mode of TE optical wave for 2 μm radius of TF with a lower n_{eff} at 1.057. In Figure 3 (d), two peaks are observed in the 2d plot signifying the higher order optic mode.

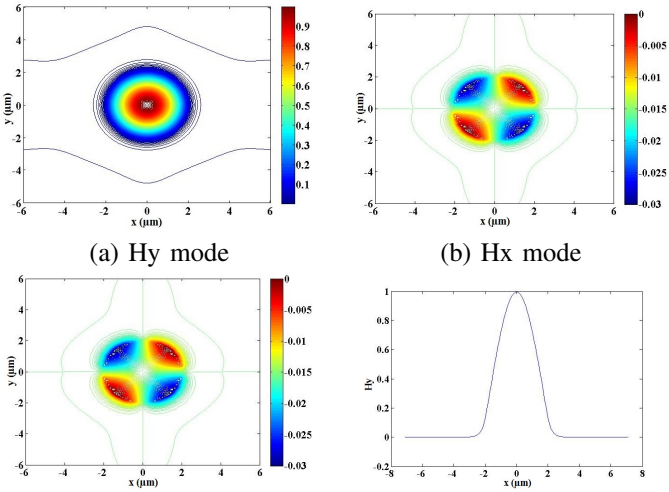

(a) Hy mode (b) Hx mode

(c) Hz mode (d) 2d plot for Hy mode

Figure 2: Fundamental optical mode for TF with R = 2 μm

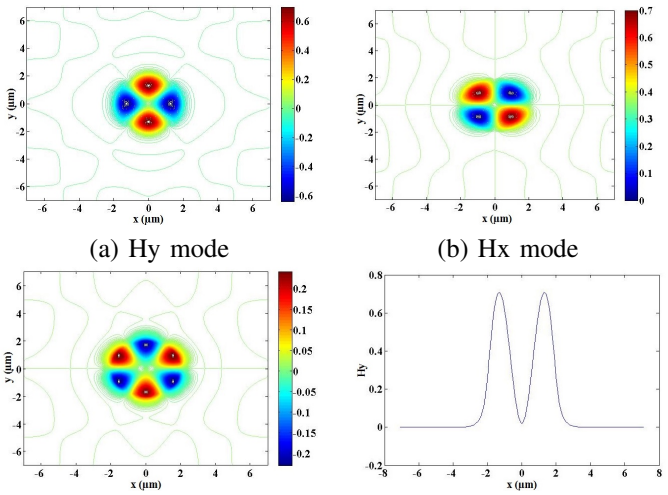

(a) Hy mode (b) Hx mode

(c) Hz mode (d) 2d plot for Hy mode

Figure 3: Higher optical mode for TF with R = 2 μm

Figure 4 shows the dominant acoustic mode in z direction. Acoustic frequency shift is at 5.26 GHz with velocity of 3306 m/s in a phase matched condition (k = 11.54 μm^{-1}). Surface acoustic velocity recorded is lower than the shear velocity (3677 m/s) and longitudinal velocity (5736 m/s). This is in agreement with the properties of SAW presented in Equation 6. SAW propagation is confirmed in Figure 4 (d) with two sharp peaks at R = 2 μm. Figure 5 shows the non-dominant acoustic mode propagating in x direction. At k = 11.54 μm^{-1}, acoustic frequency shift is at 5.633 GHz with velocity of 3338 m/s. Figure 5 (a) shows Ux mode propagation. Two sharp peaks identified at 2 and -2 signify the surface propagation. Figure 5 (b) shows Uy propagation while Figure 5 (c) shows Uz propagation. Figure 5 (d) and (e) shows 2d plot of Ux in x and y direction, respectively.

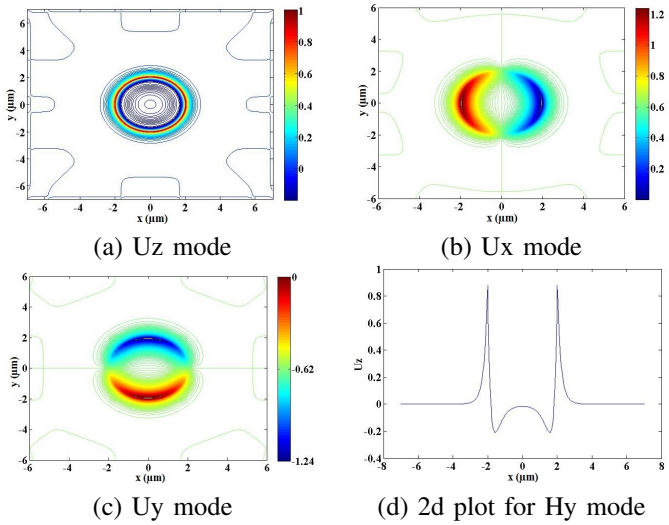

(a) Uz mode (b) Ux mode

(c) Uy mode (d) 2d plot for Hy mode

Figure 4: Dominant acoustic mode Uz for TF with R = 2 μm at phase matched condition

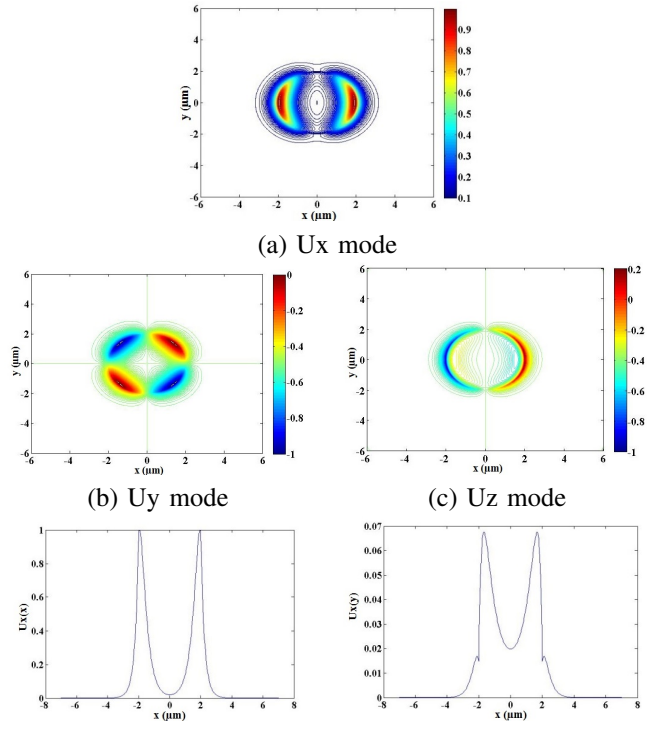

(a) Ux mode

(b) Uy mode (c) Uz mode

(d) 2d plot for Ux(x) (e) 2d plot for Ux(y)

Figure 5: Non-dominant acoustic mode Ux for TF with R = 2 μm at phase matched condition

Figure 6 plots the optic-acoustic overlapping factor versus TF core radius varies from 1 - 6 μm. Overlap integral was analyzed for 3 different wavenumbers at k = 8 μm^{-1}, k = 11.54 μm^{-1} (phase matched condition) and k = 15 μm^{-1}. For k = 8 μm^{-1}, overlap integral decreases from 0.2521 down to 0.0531. For k = 11.54 μm^{-1}, overlap integral decreases from 0.189 to 0.035. For k = 15 μm^{-1}, overlap integral decreases from 0.172 to 0.018. These findings are significant and will be useful to plot and predict the optic-acoustic overlap factor of tapered fiber under phase matched condition as well as at lower and higher k values.

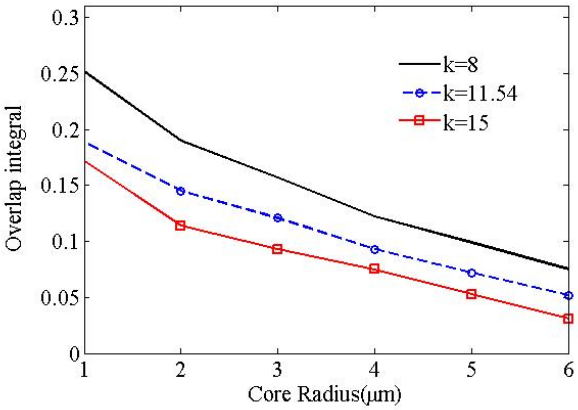

Figure 6: Overlap integral of tapered fiber vs core radius

In addition, Figure 7 shows the dominant acoustic mode Uz for R = 6 μm for phase matched condition (k = 11.54 μm^{-1}). It is observed that the surface acoustic wave (SAW) and hybrid acoustic wave (HAW) co-exist. Figure 7 records acoustic frequency shift 5.78 GHz with acoustic velocity of 3690 m/s. This modelling work successfully demonstrates the co-existence of SAW and HAW which is verified in Figure 7(d), the 2d plot for the acoustic mode propagating in the z-direction. The two sharp peaks at 6 and -6 μm signify SAW and the smooth wave confinement at fiber core represents HAW.

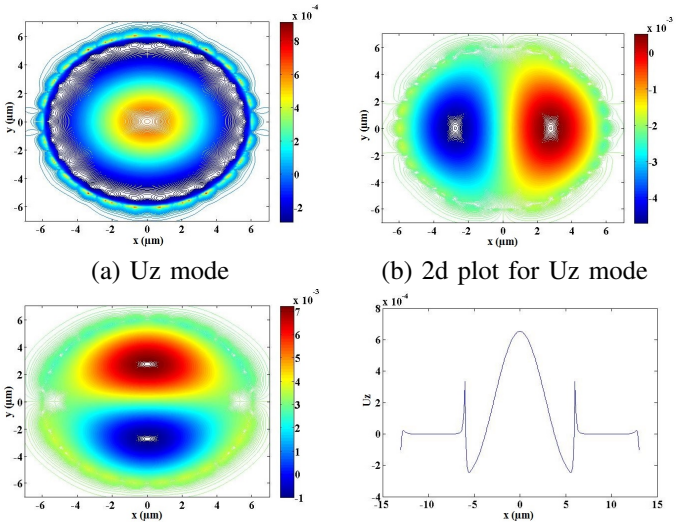

(a) Uz mode (b) 2d plot for Uz mode

(c) Ux mode (d) Uy mode

Figure 7: Dominant acoustic mode Uz for R = 6 μm under phase matched condition

V. Conclusion

The research work presents the optical and acoustic wave characterization of a 2 μm fiber at a phase matched condition for its fundamental and higher order mode wave behavior. The

overlapping factor between the optical and acoustic wave interaction for radius of 1 μm up to 6 μm are generated at three different wavenumbers of 8 μm^{-1}, phase matched condition ($11.54 \mu m^{-1}$), and 15 μm^{-1}. Lastly, the co-existence of hybrid acoustic wave and surface acoustic wave are simulated. Result shows that the numerical modeling tool can be utilized to predict the SAWs behavior of silica microfiber at different fiber radii, optical wavelengths and acoustic wavenumbers. Such finding would greatly contribute to optimize the experimental time and cost of Stimulated Brillouin Scattering.

ACKNOWLEDGMENT

The authors would like to thank Professor Azizur Rahman from City University London and Dr. Siamak Emami from Shahid Beheshti University for their guidance and UNITEN start up grant RJO10289176 for the support.

REFERENCES

[1] L. Brillouin, Diffusion de la lumière et des rayons x par un corps transparent homogène. influence de l'agitation thermique, Ann. Phys.(Paris) 17 (88-122) (1922) 21.

[2] S. Sriratanavaree, B. M. A. Rahman, D. M. H. Leung, N. Kejalakshmy, K. T. V. Grattan, Rigorous characterization of acoustic-optical interactions in silicon slot waveguides by full-vectorial finite element method, Optics Express 22 (8) (2014) 9528–9530.

[3] J. C. Beugnot, S. Lebrun, G. Pauliat, V. Laude, T. Sylvestre, Stimulated Brillouin scattering from surface acoustic waves in sub-wavelength photonic microwires 2 (2014) 1–6.

[4] C. Moreno-Hernández, D. Monzón-Hernández, I. Hernández-Romano, J. Villatoro, Single tapered fiber tip for simultaneous measurements of thickness, refractive index and distance to a sample, Opt. Express 23 (17) (2015) 22141–22148.

[5] J. Kerttula, V. Filippov, V. Ustimchik, Y. Chamorovskiy, O. G. Okhotnikov, Mode evolution in long tapered fibers with high tapering ratio, Opt. Express 20 (23) (2012) 25461–25470.

[6] A. González-Cano, M.-C. Navarrete, O. Esteban, N. Díaz-Herrera, Plasmonic Sensors Based on Doubly-Deposited Tapered Optical Fibers, Sensors 14 (3) (2014) 4791–4805.

[7] P. Wang, G. Brambilla, M. Ding, Y. Semenova, Q. Wu, G. Farrell, Investigation of single-mode;multimode;single-mode and single-mode;tapered-multimode;single-mode fiber structures and their application for refractive index sensing, J. Opt. Soc. Am. B 28 (5) (2011) 1180–1186.

[8] A. Hartung, F. Wirth, H. Bartelt, Light Propagation in Tapered Optical Fibers: Spatial Light Confinement and Generation of Plasmonic Waves, Progress In Electromagnetics Research Symposium Proceedings (2011) 255–258.

[9] T. K. Yadav, R. Narayanaswamy, M. H. Abu Bakar, Y. M. Kamil, M. a. Mahdi, Single mode tapered fiber-optic interferometer based refractive index sensor and its application to protein sensing, Optics Express 22 (19) (2014) 02–07.

[10] H. Ahmad, M. Faruki, M. Razak, Z. Tiu, M. Ismail, Evanescent field interaction of tapered fiber with graphene oxide in generation of wide-bandwidth mode-locked pulses, Optics & Laser Technology 88 (2017) 166–171.

[11] C. Sumanya, J. Comins, A. Every, Surface brillouin scattering in titanium carbide films, Wave Motion 68 (2017) 78–87.

[12] Q. Xu, W. Gao, X. Li, C. Ni, X. Chen, L. Chen, W. Zhang, J. Hu, Y. Li, M. Liao, et al., Investigation on optical and acoustic fields of stimulated brillouin scattering in as 2 s 3 suspended-core microstructured optical fibers, Optik-International Journal for Light and Electron Optics 133 (2017) 51–59.

[13] Y. Zhang, C. Yu, X. Fu, D. Li, W. Jia, W. Bi, An improved newton algorithm based on finite element analysis for extracting the brillouin scattering spectrum features, Measurement 51 (2014) 310–314.

[14] L. Murphy, Analysis of waveguides filled with uniaxial media and metamaterials for filter applications using the mode matching method, Ph.D. thesis, Syracuse University (2013).

[15] T. Asmanoglo, A. Menzel, A multi-field finite element approach for the modelling of fibre-reinforced composites with fibre-bending stiffness, Computer Methods in Applied Mechanics and Engineering.

[16] A. A. Gusev, Finite element estimates of viscoelastic stiffness of short glass fiber reinforced composites, Composite Structures 171 (2017) 53–62.

[17] O. C. Zienkiewicz, R. L. Taylor, The finite element method, Vol. 3, McGraw-hill London, 1977.

[18] Y. S. Mamdem, X. Pheron, F. Taillade, Y. Jaoüen, R. Gabet, V. Lanticq, G. Moreau, A. Boukenter, Y. Ouerdane, S. Lesoille, et al., Two-dimensional fem analysis of brillouin gain spectra in acoustic guiding and antiguiding single mode optical fibers, in: Comsol conference, 2010.

[19] Z. Zhu, D. J. Gauthier, R. W. Boyd, Stored light in an optical fiber via stimulated Brillouin scattering., Science (New York, N.Y.) 318 (5857) (2007) 1748–1750.

[20] M. R. Mokhtar, Bragg grating filters for optical networks, Ph.D. thesis, University of Southampton (2005).

[21] K. Virta, K. Mattsson, Acoustic wave propagation in complicated geometries and heterogeneous media, Journal of Scientific Computing 61 (1) (2014) 90–118.

[22] C. G. Poulton, R. Pant, B. J. Eggleton, Acoustic confinement and stimulated brillouin scattering in integrated optical waveguides, JOSA B 30 (10) (2013) 2657–2664.

[23] C. Lee, S. Chi, Measurement of stimulated-brillouin-scattering threshold for various types of fibers using brillouin optical-time-domain reflectometer, IEEE Photonics Technology Letters 12 (6) (2000) 672–674.

[24] S. Y. Yu, Q. Wang, L. Y. Zheng, C. He, X. P. Liu, M. H. Lu, Y. F. Chen, Acoustic phase-reconstruction near the dirac point of a triangular phononic crystal, Applied Physics Letters 106 (15) (2014) 115–119.

[25] V. Bansal, R. Misra, G. D. Agrawal, J. Mathur, Performance analysis of earth–pipe–air heat exchanger for summer cooling, Energy and Buildings 42 (5) (2010) 645–648.